Pharm Res (2014) 31:819–832
DOI 10.1007/s11095-013-1204-3

RESEARCH PAPER

Biomimetic Delivery Strategies at the Urothelium: Targeted Cytoinvasion in Bladder Cancer Cells via Lectin Bioconjugates

Lukas Neutsch • Britta Eggenreich • Ela Herwig • Martina Marchetti-Deschmann • Günter Allmaier • Franz Gabor • Michael Wirth

Received: 24 May 2013 / Accepted: 12 September 2013 / Published online: 24 December 2013

ABSTRACT

Purpose Urothelial cells, including bladder cancer (BCa) cells, represent a highly valuable but challenging target for localized antineoplastic therapy. This study describes a novel, biomimetic approach to improve intravesical drug delivery, based on glycan-specific targeting. In direct analogy to the invasion mechanism used by uropathogenic bacteria, we evaluate the potential of lectin bioconjugates to facilitate binding and uptake of large payload molecules at this penetration-hostile barrier.

Methods Wheat germ agglutinin (WGA) served as a targeting ligand and was covalently coupled to fluorescein-labeled bovine serum albumin (fBSA), yielding multivalent protein bioconjugates. Cytoadhesion, uptake and intracellular processing were characterized on a panel of urothelial cell lines of non-malignant and malignant origin.

Results Conjugation to WGA rendered the fBSA payload protein strongly cytoadhesive, with a clear preference in binding to cancerous cells. The highly specific, lectin-mediated recognition process was followed by rapid internalization, and extensive but non-exclusive accumulation in acid and LAMP-2-positive compartments. Stage of malignancy and mechano-structural cell configuration were important determinants for the sorting between different processing pathways.

Conclusion Lectin-bioconjugates allow for triggering endogenous uptake routes and influencing the intracellular distribution in BCa cells. They hold considerable promise for enhancing the delivery of small molecule drugs and complex biomolecules in intravesical therapy.

KEY WORDS bladder cancer · intravesical therapy · targeted drug delivery · UPEC · wheat germ agglutinin

ABBREVIATIONS

aWGA	Alexa Fluor® 594-labeled wheat germ agglutinin
BCa	Bladder cancer
bt-fBSA	Biotinylated fluorescein-labeled bovine serum albumin
DFV	Discoidal fusiform vesicles
fBSA	Fluorescein-labeled bovine serum albumin
GEMMA	Gasphase electrophoretic mobility macromolecular analysis
LAMP	Lysosome-associated membrane protein
M_1/M_2	Mander's co-localization coefficients
PCC	Pearson's correlation coefficients
RFI	Relative cell-associated fluorescence intensity
RPE	R-phycoerythrin
SEM	Standard error of the mean
UP	Uroplakin
WGA	Wheat germ agglutinin

INTRODUCTION

Bladder cancer (BCa) ranks among the most common neoplastic malignancies and, due to alerting epidemiologic trends, is counted among the deficient areas in oncology with urgent need for improvement (1,2). It mostly presents as superficial disease at the point of diagnosis, which is comparatively easy to access for surgical intervention. Successful long-term management, however, is compromised by a high tendency to recur (70%), associated with the need for frequent retreatment and cost-intensive, lifelong follow-up (3). The search for effective adjuvant strategies of

Electronic supplementary material The online version of this article (doi:10.1007/s11095-013-1204-3) contains supplementary material, which is available to authorized users.

L. Neutsch • B. Eggenreich • F. Gabor • M. Wirth (✉)
Department of Pharmaceutical Technology and Biopharmaceutics
University of Vienna, Althanstr. 14, Vienna 1090, Austria
e-mail: michael.wirth@univie.ac.at

E. Herwig • M. Marchetti-Deschmann • G. Allmaier
Institute of Chemical Technologies and Analytics
Vienna University of Technology, Getreidemarkt 9, Vienna 1060, Austria

relapse prevention has led to widespread implementation of intravesical chemo- and immunotherapy schedules into clinical practice guidelines, yet with limited impact on overall progression rates and tumor-related survival (4,5).

Next to limited exposure time, the shortcomings of lumen-borne pharmacotherapy are primarily attributed to the unique (micro-)structural and functional configuration of the human urothelium. Mechanically, drug penetration into the superficial cells is hampered by high resistance tight junctions and a semi-rigid, asymmetrical membrane (6). Dimers of a special class of transmembrane proteins, so called uroplakins (UPIa/b, UPII and UPIII), assemble to hexagonal plaques and provide a protective shielding towards the harsh intravesical environment (7). Urothelial cells show a low constitutive turnover, with a non-clathrin, non-caveolae-mediated mechanism of endocytosis that hardly includes fluid phase material (8). Moreover, several reports exist on kiss-and-run recycling of engulfing vesicles, which may cause rapid luminal resecretion of molecules that managed to circumvent the initial uptake restrictions (6,9).

Despite urgent need, comparatively little research work has so far addressed galenic modifications to improve intravesical treatment impact. Several approaches for optimizing release kinetics and prolonging the local residence time have been evaluated, including drug entrapment into particle- or hydrogel-based delivery platforms made of gelatin (10,11), chitosan (12,13), alginate (14) or other bioadhesive polymers (15–18). However, a growing body of evidence suggests that extended drug exposure alone does not lead to significant transport improvement. Rather, the resistant urothelial interface may require more specific strategies that are able to directly target molecular/functional constraints in the barrier mechanism. A prominent, nature-derived example for this strategy is the efficient invasion mechanism of uropathogenic *Escherichia Coli*, whose lectin-terminated type 1 pili allow for stable adhesion and internalization despite the harsh environmental conditions (19). A range of signaling cascades is triggered upon binding of the bacterial FimH lectin domain to (poly-)mannosylated membrane components. In further consequence, endocytic turnover is activated and certain downstream trafficking routes are redirected (20). Strikingly, such effects were also observed when applying isolated lectin molecules in absence of other bacterial invasins (6,21). Depending on their carbohydrate specificity profile, certain lectins were found to be taken up and accumulate intracellularly, yet with differences regarding the targeted compartments (21–23). At present, it is still unclear whether this route can be utilized for shuttling ligated payload across the penetration-hostile, urothelial membrane, as most data on lectin-aided internalization refer to resorptive tissues with pronounced constitutive endocytic activity (24,25). A closely related route based on targeting integrin receptors in T24 bladder cells is among the scarce examples for biorecognitive delivery strategies to be functional at this tissue (26).

Herein, we report on the successful adaption of the lectin-mediated invasion process for a second-generation delivery system that holds a binary targeting effect on the tissue/recognitive and cell biological/functional level. Our results highlight several mechanistic key parameters that should be considered when using the specific interaction with membrane-anchored carbohydrate epitopes to gain (i) preferential accumulation of lectin-ligated payload molecules at BCa cells and (ii) active sorting to receptor-triggered internalization cascades. A bioconjugate consisting of wheat germ agglutinin (WGA) and fluorescein-labeled bovine serum albumin (fBSA) served as a model vector. *Via* the fBSA/WGA conjugate, it was possible to demonstrate how known aberrances in the glycosylation of cancerous cells (27–29) may be exploited for regionally focused treatment regimens. Malignancy-associated changes in the temporal and spatial order of the lectin-triggered uptake cascade were characterized in a screening on cell lines with (5637, HT-1376) or without (SV-HUC-1) cancerous background. The endocytic processing of the bioconjugate was compared to that of the non-conjugated targeter in order to assess the impact of payload size and rule out interference with the uptake mechanism. This way, we could illustrate that the potential scope of application may include a delivery of complex biopharmaceuticals up to a size of at least 250 kDa.

MATERIALS AND METHODS

Materials

Non-modified and FITC-conjugated wheat germ agglutinin (WGA; fWGA) from *Triticum vulgare* was purchased from Vector laboratories (Burlingham, USA), Alexa Fluor® 594-labeled lectin (aWGA) from Invitrogen (Paisley, UK). Dioxane and L-glutamine were obtained from Merck (Darmstadt, GER), Superdex 200 prep grade from GE-Healthcare (Buckinghamshire, UK) and dimethylformamide from Avantor (Deventer, NL). Streptavidin conjugated with R-phycoerythrin (Streptavidin-RPE; R0438) was obtained from Dako (Glostrup, DK). Tissue culture media and supplements were acquired from Lonza (Basel, CH) and Invitrogen Ltd (Paisley, UK), respectively.

All other chemicals, including FITC-labeled albumin from bovine serum (fBSA; modified Cohn fraction V) and biotinamidocaproate N-hydroxysuccinimide ester, were obtained from Sigma-Aldrich (St. Louis, USA) and of analytical grade.

Cell Culture

The SV-HUC-1 cell line, originally established from a donor without history of urothelial malignancy, and 5637 cells, isolated from a grade 2 urothelial carcinoma, were purchased from the American Type Culture Collection (Rockville, USA). Cells were grown at 37°C in a humidified 5% CO_2/95% air atmosphere in HAM'S F-12 or RPMI 1640 medium,

respectively, supplemented with 10% FCS and antibiotics. Subcultivation followed the supplier's instructions. HT-1376 cells, established from a grade 3 BCa patient, were obtained from the Deutsche Sammlung von Mikroorganismen und Zellkulturen GmbH (Braunschweig, DE) and grown in DMEM medium supplemented with 15% FCS, 2 mM L-glutamin and antibiotics. All cells were used between passages 20–45. For monolayer experiments, cells were grown to confluency in 96-well microplates within 7–10 days after seeding (plating density 17,000 cells/well), medium was exchanged every other day. Analogously, 24,000 cells/well were seeded on glass coverslips in 24-well microplates to yield monolayer samples for high-resolution imaging.

Preparation and Physicochemical Characterization of fBSA/WGA Bioconjugates

Conjugate Synthesis and Size Fractionation

Covalent modification of the fBSA protein with lectin targeting moieties was carried out as described previously (30). Briefly, a solution of 0.5 mg fBSA (7.6 nmol) in 0.5 ml of 20 mM HEPES/NaOH pH 8.0 was added dropwise to a mixture of 0.1 ml divinyl sulfone and 0.4 ml dioxane under constant agitation, and further incubated for one hour at room temperature. Excessive divinylsulfone was removed by dialysis against the same buffer, and a 20-fold molar excess of WGA, dissolved in 1.0 ml of 20 mM HEPES/NaOH pH 8.0, was slowly added to the activated fBSA solution. This mixture was rotated end over end for at least 12 h at room temperature to let the coupling reaction proceed, yielding a panel of conjugates with different modification degrees (1–6 lectins per fBSA carrier) and free fBSA. Finally, 10 µl of a 10% (w/v) glycine solution were added to saturate unreacted coupling sites. No formation of fBSA aggregates was observed under the chosen reaction conditions, as verified by monitoring the molecular weight (see below).

The conjugate mix was fractionated *via* size exclusion chromatography over a Superdex-200® column utilizing 20 mM HEPES/NaOH pH 7.4 as an eluent; the individual fractions were characterized for molecular weight, fBSA content and coupling efficiency *via* nano-electrospray gasphase electrophoretic mobility macromolecular analysis (GEMMA) (31), PA gel electrophoresis and fluorescence spectroscopy (see Supplementary Material Table SI). Additionally, SEC fractions were subjected to an initial biological screening for cytoadhesive capacity on SV-HUC-1 cells to conclude on binding properties and determine suitable borders for product pooling (see Supplementary Material Table SI). Highly cytoaffine conjugates in the intended size range (150–250 kDa, corresponding to 2.5–5 mole WGA per mole fBSA) were isolated and pooled for further investigation; the resultant formulation was designated fBSA/WGA20. For each experiment, the fBSA/WGA20 conjugate concentration (expressed as fBSA equivalents) was adjusted to the intended level *via* a standard calibration curve for fBSA (0.0078–0.500 mg/ml; $R^2 = 0.999$) in 20 mM HEPES/NaOH pH 7.4.

Biotinylation of fBSA/WGA20 Conjugates

1.0 mg of biotinamidocaproate N-hydroxysuccinimide ester was dissolved in 1.0 ml of dimethylformamide, and 9.2 µl of this solution were mixed with 1.0 ml of purified fBSA/WGA20 conjugate solution (2.5 nmol/ml fBSA equivalents). After incubation for 1 h at room temperature under constant agitation, non-reacted ester was removed by exhaustive dialysis against isotonic 20 mM HEPES/NaOH puffer pH 7.4.

Cytoadhesion and Internalization of fBSA/WGA20 Conjugates in Urothelial Single Cells

Flow Cytometric Analysis

Surface binding and internalization in human urothelial single cells were assessed using an Epics XL-MCL analytical flow cytometer (Coulter, Miami, USA). A forward *versus* side scatter gate served to confine the analysis to the single cell population and exclude debris or cell aggregates. A minimum of 2,000 cells was accumulated for each measurement, and all experiments repeated in triplicate. The mean channel number of the logarithmic fluorescence intensities of the individual peaks was used for further calculations. All measurements were corrected for cell autofluorescence.

Concentration-Dependent Cytoadhesion

Conjugate binding capacity was assessed at 4°C, where cells are in a metabolically quiescent state and active transport processes are restricted to a minimum. Fifty µl of a pre-cooled cell suspension, containing 6.0 * 10^6 cells/ml in PBS +Ca^{2+}/Mg^{2+} (0.003 M, pH 7.2, +Ca^{2+}/Mg^{2+} at 0.001 M each), were incubated with 50 µl of conjugate solution (final concentration 0.12–2.31 nmol/ml fBSA equivalents) for 30 min (reaching a state of equilibrium). After removal of unbound conjugate *via* repeated washing and centrifugation, the cells were resuspended in 1 ml of fresh PBS + Ca^{2+}/Mg^{2+} for flow cytometric analysis of the relative cell-associated fluorescence intensity (RFI) at 488/525 nm (ex/em).

Bioconjugate Internalization

The internalization of fBSA/WGA bioconjugates was investigated in a pulse-chase experiment as described previously (30), *via* direct comparison of the pH-dependent fluorescein quench in presence or absence of active transport processes. Briefly, cells were surface-loaded with bioconjugate as described above (50 µl; 3.50 nmol/ml fBSA equivalents; 30 min 4°C), thoroughly washed, and then

incubated at either 4°C or 37°C in isotonic 20 mM HEPES/NaOH pH 7.4 for up to 120 min. At each time point, RFI was determined prior and after addition of the ionophore monensin (final concentration 1.49 μmol/ml, 4 min equilibration time), which levels the intracellular pH and thus restores the quench of the fluorescein label in acidic compartments.

Specificity of the Lectin-Mediated Cell Interaction

Single cell binding assays were repeated under competitive inhibition with highly WGA-affine N,N',N''-triacetylchitotriose in order to verify the specificity of the fBSA/WGA-cell interaction process and assess potential contributions of unspecific binding. Freshly trypsinated cells in PBS + Ca^{2+}/Mg^{2+} (25 μl containing 6.0 * 10^6 cells/ml) were added to 25 μl of isotonic 20 mM HEPES/NaOH pH 7.4 containing serial dilutions of inhibitor (0.008–2.000 mM final concentration). After incubation with 50 μl of fBSA/WGA20 conjugate solution (corresponding to 684 pmol fBSA equivalents) for 30 min at 4°C, cells were washed by centrifugation and resuspended in fresh buffer. RFI was assessed *via* flow cytometry as described above and compared to a positive control without addition of inhibitor. I_{max} and K_{I50} values were calculated on basis of a nonlinear regression fit (GraphPad Prism®, GraphPad Software Inc).

Surface Binding and Internalization of fBSA/WGA20 Bioconjugates in Urothelial Monolayers

Confluent cell layers were rinsed with isotonic 20 mM HEPES/NaOH pH 7.4, cooled to 4°C and incubated with 50 μl/well of an fBSA/WGA20 solution (450 pmol fBSA equivalents) for 30 min. After extensive washing to remove non-stably associated conjugate, cell-bound fBSA/WGA20 was quantified in an Infinite M200 fluorometer (TECAN, Gröding, Austria) at 485/525 nm (ex/em). Control samples without conjugate were analyzed in parallel to correct the values for cell autofluorescence. Next, the internalization-induced quench of the fluorophore after chase incubation for up to 90 min at 4°C and 37°C, respectively, was determined as described above. Prior to each measurement, an aliquot of the supernatant was withdrawn and analyzed at 485/525 nm (ex/em) to detect eventual release of conjugate, fBSA or free fluorophore into the surrounding medium. Again, monensin treatment (1.49 μmol/ml final conc.) was used to restore the acidic quench in late endosomal/lysosomal compartments.

Binding and Internalization of Biotinylated fBSA/WGA20 Conjugates

Time-dependent internalization of biotinylated fBSA/WGA20 conjugates, determined *via* streptavidin-RPE counterstaining, served as an alternative method to monitor endocytic uptake. Moreover, this allowed for correlating the rate of surface engulfment to endosomal/lysosomal accumulation. First, precooled cell monolayers were incubated with 50 μl of biotin-labeled fBSA/WGA20 conjugate (300 pmol fBSA equivalents in 20 mM isotonic HEPES/NaOH pH 7.4) for 30 min at 4°C, and washed with cold buffer. Cells were then, either directly or following an internalization period of up to 60 min at 37°C, counterstained with 50 μl of streptavidin-RPE (10 pmol/ml in isotonic 20 mM HEPES/NaOH pH 7.4) for 30 min at 4°C. Prior to the counterstaining, the supernatant was withdrawn and checked for fluorescence (ex/em 485/525 nm) to exclude dissociation of surface-bound conjugate during the internalization period. After thorough rinsing of the monolayers with cold buffer, cell-associated conjugate and streptavidin-RPE were quantified at 485/525 and 540/575 nm (ex/em), respectively. Control samples incubated without biotinylated conjugate were used to correct the values for endogenous streptavidin binding.

Fluorescence Microscopy and Co-localization Analysis of Bioconjugate Uptake

Imaging studies were carried out using a Zeiss Epifluorescence Axio Observer.Z1 deconvolution microscopy system (Carl Zeiss, Oberkochen, Germany) equipped with LD Plan-Neofluar objectives and the LED illumination system 'Colibri®'.

Pathway Correlation Analysis

Live single cells in suspension were imaged after settling in coverslip-mounted flexiPERM® (Greiner Bio-One, Frickenhausen, DE) chamber slides without additional fixation. The focus was set to the middle of the cell and the exposure time for each channel was kept constant to allow for direct comparison. Pulse-chase incubation was used to discriminate between the surface-bound and internalized state. The staining protocol comprised an initial loading phase of 45 min at 4°C, washing, and, if applicable, a subsequent internalization phase of 120 min at 37°C followed by a second binding phase of 45 min at 4°C. fBSA/WGA20 conjugate (25 pmol/ml fBSA equivalents) was added to the incubation medium during the first loading phase, and aWGA (25 pmol/ml) was either included in the first or in the second loading phase. A DNA-specific dye (HOECHST 33342; 5 μg/ml; Invitrogen Ltd., Paisley, UK) was added to the incubation mix for 20 min during the last step of the staining protocol to label cell nuclei. The built-in software (AxioVision 4.8.2, Carl Zeiss, Germany) was used for determining conjugate/aWGA co-localization on basis of the Pearson's correlation coefficient (PCC) and Manders' co-localization coefficients (M_1/M_2), calculated *via* the enhanced algorithm introduced by Barlow *et al.* (32). Images were processed *via* moderate iterative deconvolution and threshold values set to background mean intensity plus three times standard deviation. Data were verified by comparing in total four independent samples, with at least three imaging spots per sample.

LAMP-2 Co-localization

Cell monolayers on glass coverslips were mounted in 24 well microplates, washed, and topped with 300 µl of fBSA/WGA20 conjugate (25 pmol/ml fBSA equiv in PBS + Ca^{2+}/Mg^{2+}) for 30 min at 4°C. After thorough washing to remove unbound ligand, cells were further incubated for 60 min at 37°C or 4°C. Cells were then fixed in icecold MeOH for 15 min and rehydrated prior to immunostaining. Anti-LAMP-2 mouse monoclonal antibody (ab25631, Abcam, Cambridge UK) diluted 1:100 in PBS + Ca^{2+}/Mg^{2+}+ 1% BSA was used to label lysosomal compartments, and visualized with a rhodamine-labeled goat anti-mouse secondary antibody (ab5752, Abcam, Cambridge, UK). HOECHST 33342 DNA stain (5 µg/ml) was used to visualize cell nuclei. Co-localization of LAMP-2 and fBSA/WGA conjugates was determined using the built-in software and data processing as described above.

Statistical Analysis

RFI data were analyzed *via* one-way ANOVA and Dunnett's Multiple Comparison Test with the GraphPad Prism® software (GraphPad Software Inc.) to determine statistical significance in conjugate binding among the individual cell lines, with p-values < 0.05 considered significant.

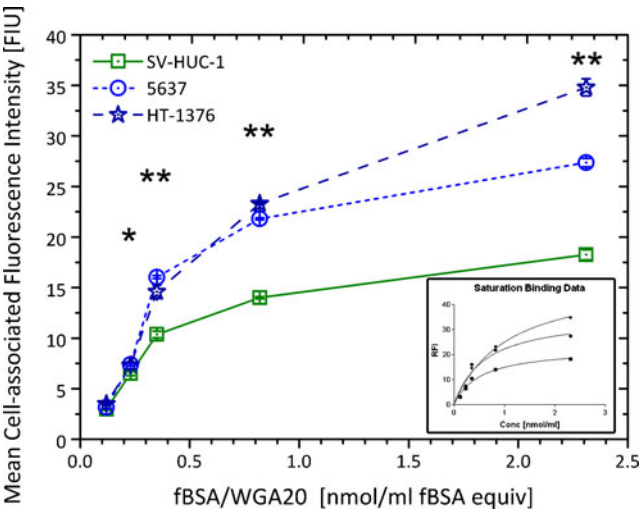

Fig. 1 Concentration-dependent cytoadhesion of fBSA/WGA20 conjugates to urothelial single cells. Freshly trypsinated cells of malignant (5637, HT-1376) or non-malignant (SV-HUC-1) origin were incubated with fBSA/WGA20 bioconjugates at various concentrations in metabolically quiescent state (4°C), washed, and analyzed by flow cytometry to determine the relative cell-associated fluorescence intensity. Data are expressed as the mean ± SEM of three independent experiments performed in triplicate, each comprising at least 2,000 cells. * and ** represent a statistically significant ($p \leq 0.05$ and $p \leq 0.01$, respectively) difference in binding capacity of both cancerous cell lines as compared to the SV-HUC-1 cell line. The *inset* shows a nonlinear regression fit ($R^2 = 0.996$, GraphPad Prism®, GraphPad Software Inc) of the binding data for estimation of saturation limits (B_{max}) and calculation of half-maximum binding concentration (K_d). RFI = relative cell-associated fluorescence intensity. Data points and axes of the inset graph correspond to those in the main graph.

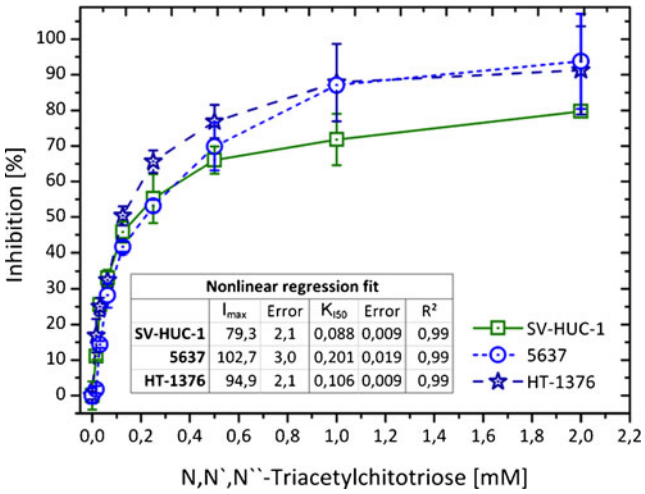

Fig. 2 Competitive inhibition of the fBSA/WGA20-cell interaction by N,N',N"-triacetylchitotriose. Single cells in suspension were incubated with fBSA/WGA20 (13.68 pmol/ml fBSA equiv) for 30 min at 4°C in presence of the complementary carbohydrate (0.000–2.000 mM final conc). Cells were washed and analyzed for cell-associated fluorescence intensity *via* flow cytometry. Values represent mean ± SEM ($n = 3$), with at least 2,000 cells per measurement. The percentage of binding inhibition refers to the cellular autofluorescence at 488/525 nm as the value for complete inhibition (100%). The *inset* shows an estimation of I_{max} (approximated maximum inhibition level) and K_{I50} (concentration for half maximum inhibition) on basis of a nonlinear regression fit (GraphPad Prism®, GraphPad Software Inc).

RESULTS

Bioconjugate Synthesis and Isolation of the Highly Affine Product Pool

The divinyl sulfone-based protocol for conjugating lectin targeters to the cargo protein allowed for fine-adjusting the average degree of modification *via* the reaction conditions, while impeding the formation of fBSA multimers or other unintended byproducts. Consistent with previous work (30), a twentyfold molar excess of lectin in the coupling reaction resulted in a mixture of bioconjugates ranging from 80 to 250 kDa in size (corresponding to up to five WGA units per fBSA), with the main fraction holding an average modification degree of 1.6 (confer Table SI in the Supplementary Material). In a preliminary screening of the size-fractionated product on urothelial SV-HUC-1 cells, the cytoadhesive capacity was found to directly correlate to the number of lectin moieties within the conjugate. Cutoff values for product pooling were set so as to collect only highly affine bioconjugates with an average WGA:fBSA ratio of 2.5 or beyond. Efficient removal of free WGA and non-modified fBSA was verified by GEMMA and PA gel electrophoresis (data not shown).

Concentration-Dependent and Cancer-Preferential Cytoadhesion on Urothelial Single Cells

As expected in case of a receptor-mediated interaction, purified fBSA/WGA20 bioconjugates adhered to the surface of

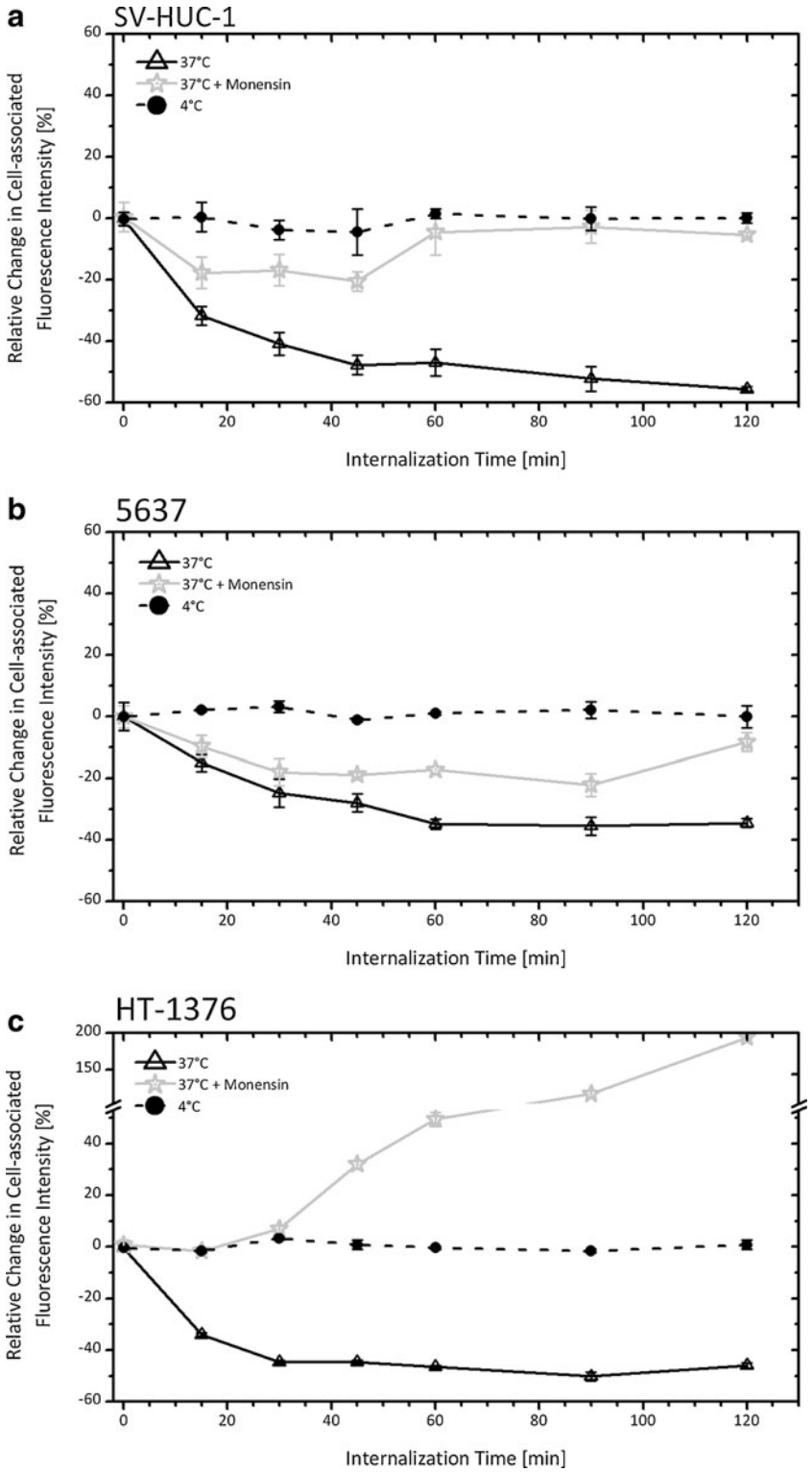

Fig. 3 Endocytic internalization of bioconjugates in urothelial single cells. Cells corresponding to (**a**) non-malignant tissue, (**b**) low grade or (**c**) high grade carcinoma were surface loaded with fBSA/WGA20 (5.8 nmol/ml fBSA equiv, 30 min, 4°C), washed, and further incubated for up to 120 min with (*37°C, solid line*) or without (*4°C, dashed line*) induction of energy-dependent transport processes. Cell-associated fluorescence intensity was determined *via* flow cytometry, and analyzed again after treatment with monensin (1.5 μmol/ml) to level intracellular pH gradients and restore the acidic quench of the fluorophore (*37°C + monensin, gray solid line*). Note the substantial increase in de-quenched fluorescence intensity in HT-1376 cells at prolonged incubation times (**c**). Values represent mean ± SEM of three independent experiments performed in triplicate and are expressed as the percental change to the initial baseline niveau after loading.

urothelial cells in a concentration-dependent manner, with gradual saturation in the range beyond 0.5 nmol/ml (Fig. 1). While no substantial differences in dependence on the stage of malignancy were observed at low concentrations, cancerous cells were found to possess a significantly ($p \leq 0.01$) higher binding saturation limit. The upward shifts in adhesion levels

obtained in the high concentration range were in good agreement with previously observed up-regulations of WGA-reactive carbohydrate moieties at advanced tumor grading (29). An approximation based on the apparent B_{max} in the nonlinear regression fit (Fig. 1 *inset*) pointed to an increase in binding capacity by a factor of 1.5 between grade 2 carcinoma cells and those derived from grade 3. Compared to SV-HUC-1 cells of non-malignant origin, this corresponds to a relative binding preference of about + 57% and + 125%, respectively. Interestingly, the shifts in the concentration required for half-maximum binding (K_D) amounted to + 17% and + 101% for 5637 and HT-1376, respectively, and thus did not directly match the relative increase in the overall loading capacity. It is thus likely that not only the amount but also the average affinity of the lectin-reactive glycan epitopes changes with malignant transformation, which may trace back to distributional shifts among the types of carbohydrate moieties involved in the binding process (*i.e.* primarily sialic acid or mono- and multimeric N-acetyl-D-glucosamine units in case of WGA). Cells incubated with non-modified fBSA served as a control and were characterized by RFI values that did not exceed the basal cell autofluorescence (0.2 ± 0.1), irrespective of their origin.

Specificity of the Biorecognitive Interaction Process

A competitive inhibition assay with N,N',N"-triacetylchitotriose was used to verify specificity of the interaction process. On all three cell lines, surface binding could be largely inhibited and only a minor portion (< 20%) was found to trace back to unspecific adsorption (Fig. 2). Final inhibition levels (I_{max} calculated *via* a nonlinear regression fit, Fig. 2 *inset*) pointed to a slightly higher tendency for unspecific adhesion on cells of non-malignant origin, which corroborated that the observed binding preference to cancerous 5637 and HT-1376 cells was indeed driven by a stronger or more extensive receptor-mediated interaction. Moreover, the concentration of N,N',N"-triacteylchitotriose required for half-maximum inhibition (K_{I50}) was twofold higher in case of 5637 cells as compared to the HT-1376 and the SV-HUC-1 cell line, giving further indication for significant differences in the affinity, and thus most probably the relative composition, of the targeted glycan pool. However, due to the dynamic interplay of type, amount and also steric accessibility of the WGA-reactive epitopes contributing to the overall conjugate-cell interaction, it is not possible to pinpoint an isolated causative factor for the differential binding behavior.

Efficient Bioconjugate Internalization and Cell-Type-Specific Downstream Processing in Urothelial Single Cells

Endocytosis of fluorescein-labeled molecules can be associated with a gradual quenching of the pH-sensitive fluorophore, caused by progressive accumulation in acidic endosomal/lysosomal compartments and other, non-pH-dependent adsorption/stacking phenomena (25). Monitoring the decrease in fluorescence intensity at 485/525 nm (ex/em) over time can thus be used for following the internalization of surface bound fBSA/WGA bioconjugates, provided an eventual loss to the surrounding medium is excluded. Upon treatment with a ionophor such as monensin, intracellular pH gradients are leveled and the quench owing to inclusion in acidic vesicles is restored. In the present study, a pulse-chase experimental setup with initial loading and a subsequent internalization phase at 4°C or 37°C was adopted in order to distinguish passive diffusion effects from energy-dependent processing.

No substantial changes in RFI were observable for cells that were chase-incubated without induction of active transport (4°C), pointing to a stable cell association mediated by the lectin targeter (Fig. 3). This was corroborated by absence of significant fluorescence levels in the supernatant over the entire test duration. Warming the cells to 37°C, in contrast, resulted in efficient conjugate internalization and related fluorescence intensity loss, with final quenching ratios amounting to 60%, 30% and 45% in case of SV-HUC-1, 5637 and HT-1376 cells, respectively. Endocytosis was found to proceed on a similar time scale for all cell lines; a steep decrease in fluorescence yield within the first 30 min was followed by gradual leveling-off, reaching a state of equilibrium at > 60 min.

Interestingly, we observed pronounced cell-type-dependent differences in the percentage of fBSA quench that was restorable *via* monensin treatment. SV-HUC-1 single cells displayed a biphasic behavior. While initially (< 60 min) 44%–59% of the intensity loss was found to be clearly pH-related, almost the entire signal (95%–97%) could be recovered at longer incubation times (Fig. 3a). A similar trend was visible in malignant 5637 cells. Here, only a minor fraction of the internalized conjugate (< 30%) seemed to be susceptible to ionophor dequenching up to 60 min after induction (Fig. 3b). However, the impact of monensin became more prominent in samples with prolonged uptake time, and at 120 min the restored fluorescence intensity amounted to 92% of the starting value. HT-1376 grade 3 carcinoma cells were characterized by a constant increase in the monensin-restorable signal, up to a final level of + 193% above the basal RFI without internalization (*4*°C, Fig. 3c). This points to a progressive proteolytic degradation of fBSA, which is known to go along with a rise in the fluorophor's signal intensity after release from the carrier protein (25,33). Of note, the pronounced increase above the 4°C baseline niveau was only visible following ionophor application, indicating that a large part of the degraded fBSA fragments was stably retained in acidic endosomal/lysosomal compartments until that point.

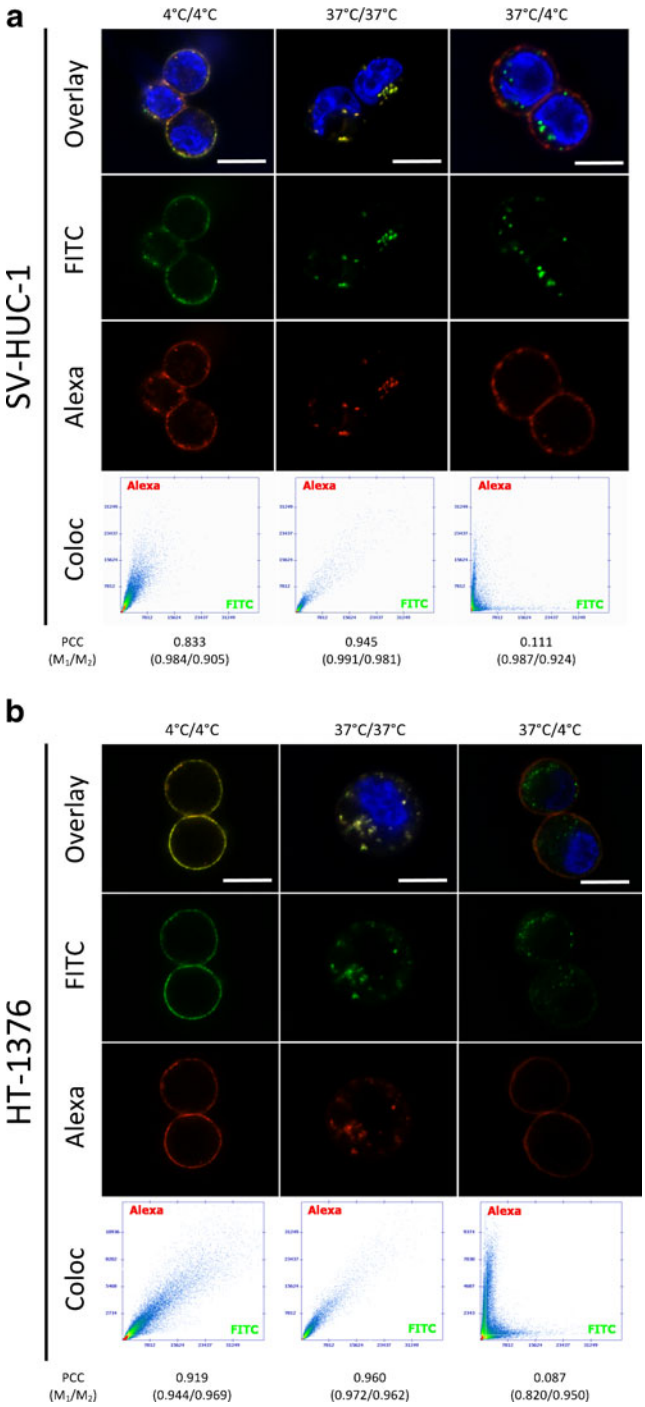

◀ **Fig. 4** Microscopic analysis of conjugate binding and internalization in urothelial single cells established from (**a**) non-malignant and (**b**) high grade BCa tissue in comparison to the non-conjugated lectin targeter (aWGA). Images show merged channels with Hoechst 33342 DNA stain (*Overlay*), or the individual channels for the conjugate's fluorescein label (*FITC*) and Alexa Fluor® 594 labeled WGA (*Alexa*). In metabolically quiescent state (loading for 45 min at 4°C), co-incubation of fBSA/WGA20 and aWGA results in mere staining of the cell surface (*4°C/4°C*). Energy-dependent endocytosis of fBSA/WGA20 conjugates is visible by clear intracellular clustering (45 min loading at 4°C, followed by 120 min of internalization at 37°C), and produces identical staining patterns if aWGA is applied in parallel (*37°C/37°C*). If aWGA is applied in a subsequent incubation step under reduced metabolic turnover (loading at 4°C 45 min, incubation for 120 min at 37°C, cooling to 4°C and aWGA post-incubation for 45 min) internalized fBSA/WGA20 can be clearly distinguished from the aWGA stain at the surface (*37°C/4°C*). Images were captured using identical exposure conditions to allow for direct comparison. Scale bar = 10 μm. Co-localization analysis shows Pearson's correlation coefficients (PCC) and Mander's co-localization coefficients (M_1/M_2) for the above overlays, together with the respective scatter plots.

Congruent Uptake Pathway(s) for Surface-Bound Lectins and Lectin-Bioconjugates Despite Substantially Increased Molecular Weight

Efficient, lectin-triggered uptake could be qualitatively confirmed *via* simultaneous or sequential incubation/internalization of fBSA/WGA20 conjugates and the free, Alexa594-labeled targeter (aWGA; Fig. 4). The staining pattern of both labels was confined to the outer membrane when incubated at 4°C. Upon warming to 37°C, a decrease in staining intensity at the surface and concomitant clustering, first in membrane-proximal and then in cytoplasmatic compartments, became visible (confer also Figure S1 in the Supplementary Material for time-lapse imaging of the uptake process). Free lectin and the lectin-modified conjugate exhibited a high parallelism in the endocytic processing cascade, as indicated by a near-complete co-localization (PCC of 0.945 for SV-HUC-1 and 0.960 for HT-1376, respectively, after simultaneous application). In contrast, sequential binding/uptake/binding-assays with conjugate internalization (37°C) being followed by aWGA surface labeling (4°C) resulted in a PCC of only 0.111 and 0.087, respectively. This low degree of co-localization indicates that large portions of conjugate were already engulfed from the surface and translocated to downstream organelles after 60 min of incubation, corroborating the data from quantitative uptake studies.

In all cell lines, a slightly lower degree of aWGA/bioconjugate co-localization after concomitant surface loading (4°C/4°C) was visible and pointed to differences in the receptor pool that is targeted by the multivalent conjugate and the free ligand. However, these differences seem to remain without further consequences for downstream processing, indicated by the near-complete colocalzation upon activation of energy-dependent turnover. This effect was also visible in monolayer samples (confer Figure S1 in the Supplementary Material).

Mechanostructural Differences Between Single Cell and Monolayer Configuration Are Irrelevant for Surface Adhesion but Can Alter Degradative Capacity

Treatment success of intravesical chemotherapy critically depends on an adequate drug impact on both, mechanically detached cancer cells in the lumen that may re-implant in the bladder lining after surgery as well as non-resected tumor tissue

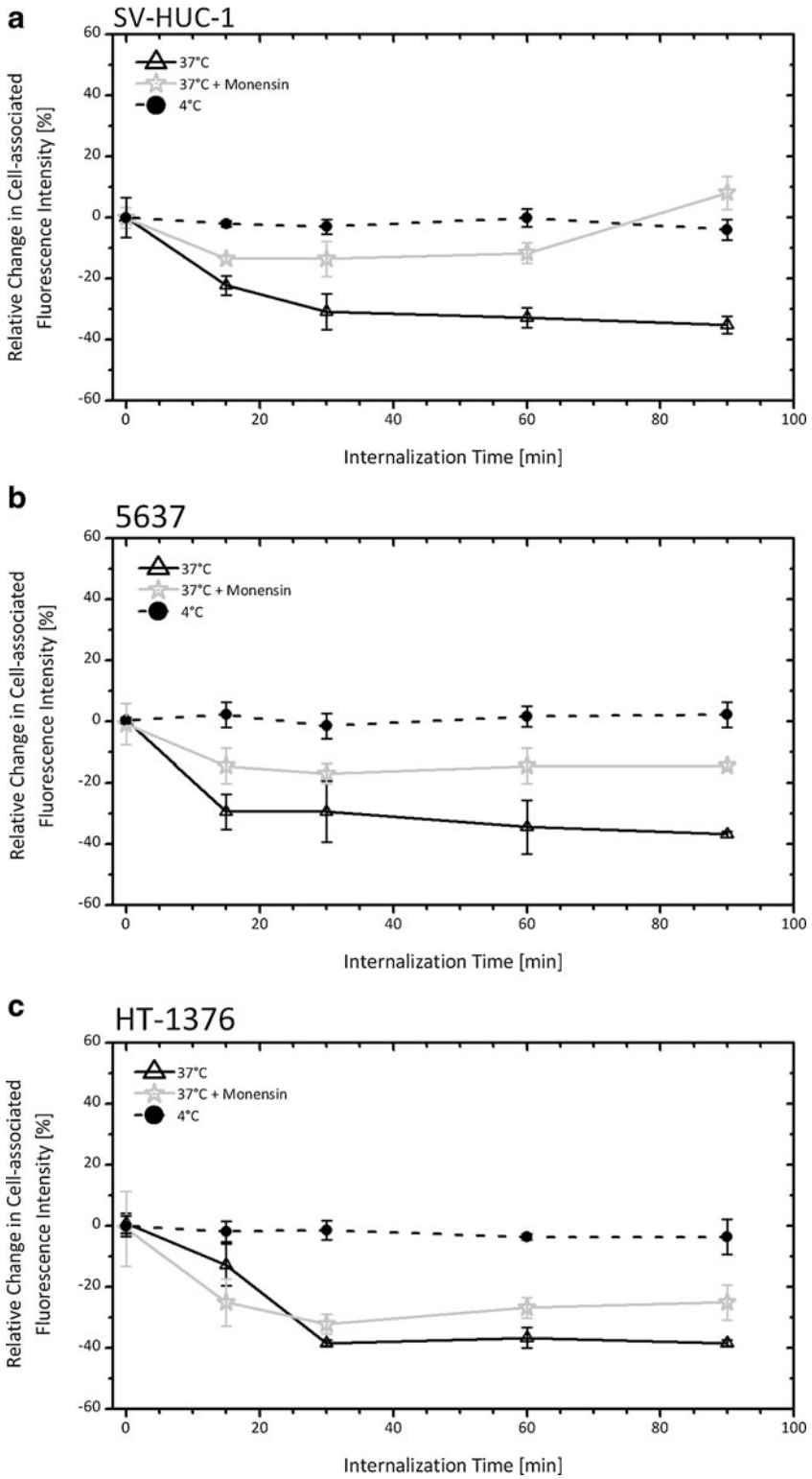

Fig. 5 Endocytic internalization of bioconjugates in urothelial monolayers corresponding to (**a**) non-malignant tissue, (**b**) low grade or (**c**) high grade carcinoma. Confluent cell monolayers were surface loaded with fBSA/WGA20 (9.0 nmol/ml fBSA equiv, 30 min, 4°C), washed, and further incubated for up to 90 min with (*37°C, solid line*) or without (*4°C, dashed line*) induction of energy-dependent transport processes. Stably cell-associated fBSA was quantified *via* fluorescence readout (ex/em: 485/525 nm) and analyzed again after treatment with monensin (1.5 μmol/ml) to level intracellular pH gradients and restore the acidic quench of the fluorophore in endosomal/lysosomal compartments (*37°C + monensin*, gray solid line). Values represent the mean ± SEM of three independent experiments performed in quadruplicate and are expressed as the percental change to the initial baseline niveau after loading.

left at the site of disease. Potent intravesical delivery vehicles thus need to mediate efficient uptake in cells under both structural configurations. However, due to cell polarization and other effects, the intact tissue organization may differ from the isolated state with regard to surface exposure and/or accessibility of certain glycoproteins and glycolipids. Binding levels as well as further processing cascades may be altered in response, with direct implication for receptor-mediated targeting strategies.

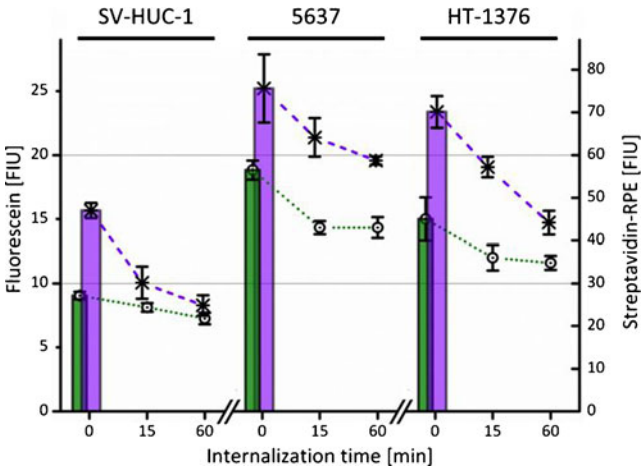

Fig. 6 Simultaneous analysis of surface engulfment and endosomal/lysosomal accumulation of biotinylated conjugates. Confluent monolayer samples of urothelial cells, corresponding to different malignant gradings, were cooled to 4°C, surface loaded with biotinylated fBSA/WGA20 (6.0 nmol/ml fBSA equiv, 4°C, 30 min), washed, and chase-incubated for up to 60 min at 37°C. Non-quenched, cell-associated fluorescein levels were determined *via* read-out at 485/525 nm (ex/em; *green bars*) and surface-accessible conjugates were quantified by a streptavidin-RPE counterstaining (*purple bars*), allowing for a direct comparison of removal from the surface to quenching in acidic compartments. Data represent means ± SEM of three independent experiments. Values were corrected for cell autofluorescence and basal streptavidin binding, control measurements in the supernatant served to rule out conjugate dissociation from the surface during the incubation period.

For the here established glycotargeted delivery vector, the binding capacity of monolayer samples matched the trend found in single cell state; under saturated conditions, the relative amount of stably associated fBSA/WGA20 on cancerous cells exceeded that on SV-HUC-1 by 108.1 ± 7.2% (5637) and 65.8 ± 14.5% (HT-1376), respectively. However, cell type-dependent differences in conjugate internalization were less pronounced when in confluent tissue configuration, as illustrated by a rather uniform quenching ratio of 35–38% for all cell lines (Fig. 5). Again, no change in RFI was observed when active transport was inhibited (*4*°C). Bioconjugate dissociation into the supernatant proved to be negligible throughout the experiment.

Response rates to ionophor treatment varied among the individual cell lines also in monolayer samples, and, moreover, exhibited substantial differences as compared to the single cell state. Most notably, high-grade HT-1376 carcinoma cells did not show rapid onset of proteolytic conjugate degradation (Fig. 5c). A signal fraction of no more than 35% was found to be susceptible to pH-leveling, indicating that intracellular conjugate trafficking or the metabolic activity of engulfing vesicles changed substantially in response to the altered mechano-structural configuration. Slightly higher dequenching levels were observed for 5637 cells (42–61%, Fig. 5b), roughly equivalent to those in single cell state, and non-malignant SV-HUC-1 monolayers exhibited the most notable monensin response with a restored fluorescence intensity exceeding the 4°C baseline niveau at an internalization time >60 min (Fig. 5a).

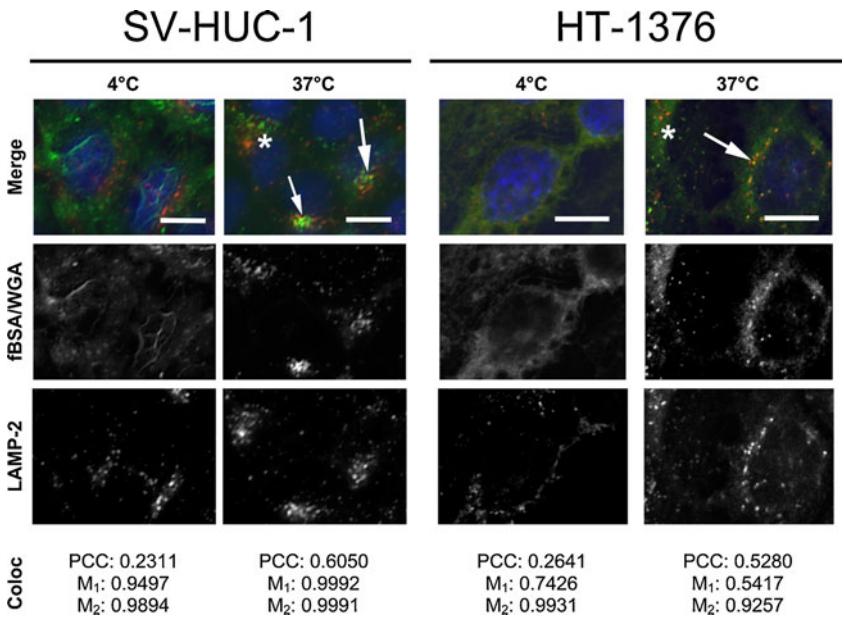

Fig. 7 Partial lysosomal accumulation of fBSA/WGA20 bioconjugates in urothelial monolayers. Non-malignant SV-HUC1 and cancerous HT-1376 cells were incubated with fBSA/WGA20 according to a pulse-chase protocol with or without induction of active transport (30 min loading at 4°C, 60 min of incubation at 4°C or 37°C). After fixation (icecold MeOH) and rehydration in buffer, LAMP-2-positive compartments were visualized immunohistochemically using a rhodamine-labeled secondary antibody. Merged images show an overlay of the individual channels with an additional Hoechst 33342 nuclei stain. Exemplary areas with marked LAMP-2/bioconjugate co-localization are designated by *arrows*, *asterisks* denote examples of non-overlapping regions. Scale bar = 10 μm. fBSA/WGA co-localization was determined by calculating Pearson's correlation coefficients (PCC) and Mander's co-localization coefficients (M_1/M_2) for the above overlays. Images shown are representative for six fields of view analyzed in three independent samples.

Simultaneous Activation of Diverse Endocytic Pathways

For a more detailed characterization of the uptake process, surface binding and engulfment of biotinylated conjugates (bt-fBSA/WGA) were quantified *via* streptavidin counterstaining and correlated to the rate of acidic quenching. Results were corrected for constitutive RPE-streptavidin binding and control measurements in the supernatant served to rule out conjugate dissociation from the surface. Biotinylated conjugates displayed the same cancer-preferential adhesion profile as the pristine fBSA/WGA conjugate (Fig. 6), suggesting that the subsequent modification with biotin/spacer-groups did not interfere with the specific lectin-cell interaction, *e.g.* by blocking the carbohydrate binding domain. The fraction of apically exposed biotin moieties decreased concomitantly to the loss in fBSA fluorescence, yet on a comparatively higher relative scale. For SV-HUC-1 cells, a decrease of 47.2±13.1% in the streptavidin-accessible biotin units after 60 min was correlated to a fluorescein quench of only 19.9±8.7% after the same time. Similar trends were found for cancerous cell lines, pointing to a more or less pronounced lag phase between membrane endocytosis and translocation to acidic endosomes/lysosomes, or respectively, simultaneous accumulation in organelles without progressive acidification.

Partial Accumulation of Bioconjugates in LAMP-2-Positive Compartments

Immunofluorescence analysis of bioconjugate uptake in monolayer samples qualitatively corroborated the simultaneous sorting to different pathways by showing only partial co-localization (PCC: 0.5–0.6, Fig. 7) to the lysosome marker LAMP-2 after 60 min of internalization. According to quenching data (Fig. 5), translocation to acidic compartments should be largely completed at this point. Again, an initially homogenous surface stain of the bioconjugate after loading changed into a cluster-like appearance after initiating energy-dependent turnover. The accumulating vesicles primarily localized to the perinuclear region, and both, LAMP-2-negative conjugate-rich clusters as well as lysosomal compartments without conjugate loading were visible next to the overlapping portion. No significant differences in the degree of lysosome accumulation were found between the individual cell lines.

DISCUSSION

Cells of urothelial origin display a penetration-hostile functional and mechanical configuration, with only minimal access to endocytic uptake routes from the apical side (6,8,21). However, the FimH-mediated bacterial cytoinvasion, triggered by adhesion to polymannosylated glycoproteins and localized membrane/cytoskeleton reorganization, provides a prominent example of how to utilize the cellular machinery for bypassing the endogenous permeability restrictions (19,20). In the present work, we sought to clarify whether WGA, a readily available plant lectin, can be utilized to mimick the mannose-directed invasion process of FimH with glycan epitopes that show a disease-modulated distribution pattern. *In vivo*, this may not only allow for increased intravesical residence time but also facilitate preferential accumulation in cancerous areas. Importantly, in order to be of clinical use, receptor interaction and efficient sorting to endocytic uptake must be possible with an API attached to the targeting ligand.

We found the dimeric WGA lectin to be suitable for direct covalent conjugation without additional linkers and to retain its high cytoadhesive potential and discrimination capability (30) despite the covalent attachment to a larger sized payload protein. This applied to all of the fBSA/WGA model bioconjugates tested in this study. In future application, also the activity of the conjugated API or payload protein will need to be monitored and eventually optimized to ensure therapeutic efficacy. Depending on the specific application, this may involve acid-sensitive linkers or similar triggered-cleavage systems.

The preferential binding on cancerous cells most likely grounds in a combination of numerical and affinity-related shifts in the pool of accessible glycoproteins/-lipids. While of variable extent for single cell and monolayer samples, increased adhesion to BCa cells could be confirmed under both configurations (Figs. 1 and 6). Thus, as a key aspect of this work, we demonstrate that the previously observed aberrant glycosylation of urothelial cells (27,28) and/or alternative modulations in the pattern of surface-accessible carbohydrates may actually be utilized for establishing regionally focused treatment strategies.

The exact fate of internalized membrane and adherent/associated ligands in urothelial cells is still an unresolved question. In analogy to other epithelia, the specific receptors engaged upon surface binding have been shown to be of decisive influence for the efficient sorting to entry pathways and further intracellular processing (8,22,34). Normally, caveolae- and clathrin-independent mechanisms seem to dominate endocytic membrane traffic in fully differentiated urothelium (8), but biorecognitive binding may also trigger alternative routes without constitutive activity. So far, integrin- (19,26), AP-2 adaptor protein- (35), and uroplakin-dependent (6) stimuli were described among the effectors of uptake cascades, including those triggered by the FimH lectin domain. At least two major processing pathways are available once the material is internalized, one corresponding to the classical endosomal/lysosomal degradation route with – non-mandatory – transit through multivesicular early endosomes, and the other involving transient or durable entrapment in specific discoidal fusiform vesicles (DFV). The latter belong to the class of secretory lysosomes, which are characterized by an acidified lumen but lack pronounced degradative capacity (6,9,36), DFVs are rich in uroplakin 3a, one of the few clearly identified WGA-reactive

glycoproteins in the urothelial membrane (34), and may thus belong to the primary targets of the fBSA/WGA bioconjugates. From there, they may either be further translocated to lysosomes or be subjected to luminal re-exocytosis (6,9,37).

The efficient internalization with ample pH-related quenching observed in the present study goes in accordance with the canonical trafficking model. In single cell state, quenching ratios (30–60%) were inversely correlated to the overall binding capacity of the cell line (Figs. 1 and 3). Monolayer samples, in contrast, though exhibiting a similar tumor-preferential binding pattern (Fig. 6), were characterized by a rather uniform quench between 30 and 40% of the total pool of surface-bound fBSA/WGA (Fig. 5). With regard to the initial surface load, this means that in cancerous monolayers a higher net amount of fBSA/WGA was accumulated in quenching compartments as compared to the non-malignant SV-HUC-1 monolayers. An important message with regard to biorecognitive delivery shuttles at the urothelium thus is that an increased surface binding of the targeter is likely to (monolayer state), but may not necessarily (single state), translate into higher endosomal uptake rates of the conjugated payload. Note that the percental endosomal uptake ratio of the fBSA/WGA bioconjugates in all cells closely matched the uptake characteristics observed for the free WGA lectin alone (29). This indicates that the largest portion of lectin targeter retained its active configuration after fBSA conjugation, with unimpeded binding affinity.

Substantial cell-type-related differences in the signal response upon pH leveling, as *e.g.* observed between low- and high-grade carcinoma single cells (Fig. 3b, c), suggest the existence of more than one main processing route for the internalized payload. Each may transfer the conjugate to acidic compartments at a different rate. All involved routes seemed to include, to a larger or minor extent, fBSA clustering at sites with high local fluorophore densities, which are not completely de-quenchable by neutralization. Respective effects were observed as early as 15 min after induction of active transport (Figs. 3 and 5). The comparatively more rapid onset of degradative processes in HT-1376 single cells (Fig. 3c) may trace back to higher transport efficiency in the cytoplasmatic compartment, higher metabolic activity of the proteolytic organelles or a relative predominance of the lysosomal processing route with regard to other pathways in this cell line. Earlier studies have reported a grade-dependent up-regulation of caveolin-1 and 2, two key proteins of lipid-raft internalization, in BCa cells (38). This may hypothetically lead to faster uptake and/or translocation to lysosomes in high-grade cells, but a causal relation remains yet to be clarified. Given the additional, profound impact of the cells' mechanical configuration on the rate of conjugate degradation, which was most evident in direct comparison of HT-1376 single cells to monolayer samples (Figs. 3c and 5c), a decisive role of structural/trafficking-related factors is likely. Controlled actin filament rearrangements, altering membrane tension and the cytoskeletal organization, were identified as a key regulator of FimH-mediated cytoinvasion in the urothelium (8,20). Similar effects can result from architectural changes between the single cell and monolayer state, and might account for the differential processing. It is, however, important to note that also changes in the glycan receptor pool at the surface were shown to have consequences for the extent of the bacterial, lectin-mediated cell invasion (39). Hence, the causative trigger point for distinct WGA-conjugate trafficking may already lie prior to the engulfment process *per se* and thereby be highly sensitive to alterations in the biorecognitive interaction for each cell line and tissue configuration. Of immediate relevance for targeted delivery applications, we conclude that a cytoadhesive ligand on the urothelium should be carfully evaluated for its influence on rate and extent of internalization, as well as on the downstream processing of the delivered payload. *Vice versa*, careful selection may allow for preferential translocation to the intended target organelle(s).

Another important aspect revealed by the analysis of conjugate fate after internalization is that, irrespective of the cells' degradative capacity, the fluorescence quench remained on a stable level prior to monensin treatment. This suggests that both fBSA/WGA conjugates as well as potential smaller degradation fragments were durably entrapped in the engulfing compartments, and, contrasting to other reports on incorporated material in BCa cells, not subjected to rapid re-exocytosis (9). In clinical application, this may offer a potent strategy for bypassing resistance mechanisms caused by active recycling. Some studies reported constitutive membrane pinch-off in bladder tissue (37), which naturally could limit the efficacy of any bioadhesive targeting vector at the urothelium. However, we found no substantial loss of surface-bound conjugate over the test period, and thus hypothesize that either (i) pinch-off events were of minor importance in the present cell model or (ii) the rapid internalization of glycan-bound bioconjugates from the surface impeded extensive loss with secreted membrane segments.

In general, conjugates internalized in monolayers seemed to face a relatively mild environment, without ample degradation in the investigated time frame of up to 90 min (Fig. 5). Our observation of only partial lysosomal accumulation goes in direct concordance to previous uptake studies at mechanically stimulated urothelium (34), which found fWGA and LAMP-2 to colocalize to a very similar extent (PCC of ~0.6). However, while in our study (steady state) both fBSA/WGA and the free targeter (aWGA) primarily accumulated in compartments lying in the perinuclear region (Figs. 4, 7 and SI1), assays under mechanical stimulation reported clustering in rather peripheral compartments close to the cell border. Thus, it is likely that despite attachment to similar binding epitopes, other, or additional endocytic mechanisms are activated upon mechanical stimulation, associated with a change in trafficking and terminal accumulation in differentially localized but functionally analogous organelles.

The direct quantification of conjugate engulfment *via* biotin/streptavidin counterstaining provided an alternative means for characterizing the internalization process and pointed out that quenching-based endocytosis ratios should be regarded a minimum value for actual uptake (Fig. 6). In particular, we found surface endocytosis to continue at an only slightly reduced rate, while accumulation in organelles/at sites with acidic or intermolecular fBSA quenching stagnated after the first 15 min of incubation. It is thus reasonable to assume that the limiting bottleneck for conjugate transfer to acidic or densely packed (quenching) compartments is located downstream of the engulfment mechanism *per se*. Besides, a continuously ongoing processing *via* an alternative pathway without acidification, and without early onset of saturation effects, cannot be ruled out. Seen in combination with the ample but not exclusive LAMP-2 co-localization (Fig. 7), a considerable fraction of payload molecules seems to be entrapped without exposure to a degradative environment, holding promise that also fragile biopharmaceuticals may successfully be delivered *via* the lectin-triggered uptake route(s).

One caveat associated with *in vitro* uptake assays on urothelium is that cultured cells are known to reside at a lower stage of differentiation as compared to the native environment, which may lead to potential overestimation of the endocytic capacity (40). More comprehensive studies in the clinical setting will be required to allow for a definite statement on the impact of environmental factors on the efficacy of carbohydrate-triggered internalization processes. However, based on the high parallelism in processing routes of WGA conjugates and free fWGA *in vitro*, it is likely that also in the intact physiological niche lectin-modified prodrugs will share similar pathways with the non-conjugated targeter. Thus, reports on the ample uptake of the WGA targeter itself in animal studies (6,8) may be seen as a promising predictive indicator for efficient bioconjugate internalization in the *in vivo* state. Similar animal studies, including tumor models, would present a highly valuable tool for initial conclusions on bioconjugate functionality. However, the cell glycosylation pattern of the animal host has to be carefully analyzed for aberrances with regard to human tissue in order to allow for direct comparison.

CONCLUSION

With regard to the unmet need for improved treatment modalities in intravesical therapy, our study aimed at evaluating the largely unexplored potential of biorecognitive delivery vectors to urothelial cells. We were able to show that the mannose-directed invasion of Fim-H piliated bacteria can be adapted to WGA-reactive carbohydrates, which, due to a relatively higher abundance in malignant cells, can serve as promising targeting epitopes for preferential internalization of large molecular weight payload in BCa tissue. The specific interaction potential mediated by the lectin was identified as a key trigger for efficient uptake and could be transferred to the model payload *via* direct covalent conjugation without negatively impacting endocytic uptake or downstream processing. WGA-induced internalization resulted in substantial, but not exclusive, terminal accumulation in degradative lysosomal compartments. By establishing an end-to-end causal connection between glycorecognitive binding and stable intracellular entrapment, our results provide a valuable preliminary framework for future exploitation of aberrant BCa cell glycosylation in targeted delivery applications. Physicochemical characteristics of the bioconjugate (*e.g.*, modification degree), specificity to chosen carbohydrate epitopes as well as the structural configuration of the target cells need to be considered as important influencing variables in the development of biomolecularly targeted strategies for the intravesical route and are subject of continuing investigation.

ASSOCIATED CONTENT

Supplemental data and experimental methods on the physicochemical and initial biological characterization of the conjugate fractions from SEC with a calculation of the normalized cytoadhesive capacity (Table SI) are available in the Supplementary Material. Figure S1 shows a more detailed time-lapse study of bioconjugate uptake in 5637 single cells. Co-localization of fBSA/WGA with the free targeting ligand (aWGA) in SV-HUC-1 monolayers prior and after internalization can be taken from Figure S2.

REFERENCES

1. Kamel MH, Moore PC, Bissada NK, Heshmat SM. Potential years of life lost due to urogenital cancer in the United States: trends from 1972 to 2006 based on data from the SEER database. J Urol. 2012;187:868–71.
2. Sievert KD, Amend B, Nagele U, Schilling D, Bedke J, Horstmann M, *et al*. Economic aspects of bladder cancer: what are the benefits and costs? World J Urol. 2009;27:295–300.
3. van Rhijn BW, Burger M, Lotan Y, Solsona E, Stief CG, Sylvester RJ, *et al*. Recurrence and progression of disease in non-muscle-invasive bladder cancer: from epidemiology to treatment strategy. Eur Urol. 2009;56:430–42.
4. Shen Z, Shen T, Wientjes MG, O'Donnell MA, Au JL. Intravesical treatments of bladder cancer: review. Pharm Res. 2008;25:1500–10.
5. Witjesand JA, Hendricksen K. Intravesical pharmacotherapy for non-muscle-invasive bladder cancer: a critical analysis of currently available drugs, treatment schedules, and long-term results. Eur Urol. 2008;53:45–52.
6. Khandelwal P, Abraham SN, Apodaca G. Cell biology and physiology of the uroepithelium. Am J Physiol Ren Physiol. 2009;297:F1477–501.
7. Wu XR, Kong XP, Pellicer A, Kreibich G, Sun TT. Uroplakins in urothelial biology, function, and disease. Kidney Int. 2009;75:1153–65.

8. Kreft ME, Jezernik K, Kreft M, Romih R. Apical plasma membrane traffic in superficial cells of bladder urothelium. Ann N Y Acad Sci. 2009;1152:18–29.
9. Bishop BL, Duncan MJ, Song J, Li G, Zaas D, Abraham SN. Cyclic AMP-regulated exocytosis of Escherichia coli from infected bladder epithelial cells. Nat Med. 2007;13:625–30.
10. Lu Z, Yeh TK, Tsai M, Au JL, Wientjes MG. Paclitaxel-loaded gelatin nanoparticles for intravesical bladder cancer therapy. Clin Cancer Res Off J Am Assoc Cancer Res. 2004;10:7677–84.
11. Chen JP, Leu YL, Fang CL, Chen CH, Fang JY. Thermosensitive hydrogels composed of hyaluronic acid and gelatin as carriers for the intravesical administration of cisplatin. J Pharm Sci. 2011;100:655–66.
12. Barthelmes J, Perera G, Hombach J, Dunnhaupt S, Bernkop-Schnurch A. Development of a mucoadhesive nanoparticulate drug delivery system for a targeted drug release in the bladder. Int J Pharm. 2011;416:339–45.
13. Bilensoy E, Sarisozen C, Esendagli G, Dogan AL, Aktas Y, Sen M, *et al*. Intravesical cationic nanoparticles of chitosan and polycaprolactone for the delivery of Mitomycin C to bladder tumors. Int J Pharm. 2009;371:170–6.
14. Denkbas EB, Ozdemyr N, Ozturk E, Eroglu M, Acar A. Mitomycin-C-loaded alginate carriers for bladder cancer chemotherapy. J Bioact Compat Polym. 2004;19:33–44.
15. Chang LC, Wu SC, Tsai JW, Yu TJ, Tsai TR. Optimization of epirubicin nanoparticles using experimental design for enhanced intravesical drug delivery. Int J Pharm. 2009;376:195–203.
16. Le Visage C, Rioux-Leclercq N, Haller M, Breton P, Malavaud B, Leong K. Efficacy of paclitaxel released from bio-adhesive polymer microspheres on model superficial bladder cancer. J Urol. 2004;171: 1324–9.
17. Mugabe C, Matsui Y, So AI, Gleave ME, Baker JH, Minchinton AI, *et al*. In vivo evaluation of mucoadhesive nanoparticulate docetaxel for intravesical treatment of non-muscle-invasive bladder cancer. Clin Cancer Res Off J Am Assoc Cancer Res. 2011;17:2788–98.
18. Tyagi P, Li Z, Chancellor M, De Groat WC, Yoshimura N, Huang L. Sustained intravesical drug delivery using thermosensitive hydrogel. Pharm Res. 2004;21:832–7.
19. Eto DS, Jones TA, Sundsbak JL, Mulvey MA. Integrin-mediated host cell invasion by type 1-piliated uropathogenic Escherichia coli. PLoS Pathog. 2007;3:e100.
20. Dhakal BK, Kulesus RR, Mulvey MA. Mechanisms and consequences of bladder cell invasion by uropathogenic Escherichia coli. Eur J Clin Investig. 2008;38 Suppl 2:2–11.
21. Truschel ST, Wang E, Ruiz WG, Leung SM, Rojas R, Lavelle J, *et al*. Stretch-regulated exocytosis/endocytosis in bladder umbrella cells. Mol Biol Cell. 2002;13:830–46.
22. Yi SMP, Harson RE, Zabner J, Welsh MJ. Lectin binding and endocytosis at the apical surface of human airway epithelia. Gene Ther. 2001;8:1826–32.
23. Lehr CM. Lectin-mediated drug delivery: the second generation of bioadhesives. J Control Release Off J Control Release Soc. 2000;65: 19–29.
24. Haltner E, Easson JH, Lehr C-M. Lectins and bacterial invasion factors for controlling endo- and transcytosis of bioadhesive drug carrier systems. Eur J Pharm Biopharm Off J Arbeitsgemeinschaft Pharm Verfahrenstechnik eV. 1997;44:3–13.
25. Gabor F, Schwarzbauer A, Wirth M. Lectin-mediated drug delivery: binding and uptake of BSA-WGA conjugates using the Caco-2 model. Int J Pharm. 2002;237:227–39.
26. Coon BG, Crist S, Gonzalez-Bonet AM, Kim HK, Sowa J, Thompson DH, *et al*. Fibronectin attachment protein from bacillus Calmette-Guerin as targeting agent for bladder tumor cells. Int J Cancer. 2012;131:591–600.
27. Ohyama C. Glycosylation in bladder cancer. Int J Clin Oncol/Jpn Soc Clin Oncol. 2008;13:308–13.
28. Neal DE, Charlton RG, Bennett MK. Histochemical study of lectin binding in neoplastic and non-neoplastic urothelium. Br J Urol. 1987;60:399–404.
29. Neutsch L, Plattner VE, Polster-Wildhofen S, Zidar A, Chott A, Borchard G, *et al*. Lectin mediated biorecognition as a novel strategy for targeted delivery to bladder cancer. J Urol. 2011;186:1481–8.
30. Neutsch L, Eggenreich B, Herwig E, Marchetti-Deschmann M, Allmaier G, Gabor F, *et al*. Lectin bioconjugates trigger urothelial cytoinvasion - A glycotargeted approach for improved intravesical drug delivery. Eur J Pharm Biopharm Off J Arbeitsgemeinschaft Pharm Verfahrenstechnik eV. 2012;82:367–75.
31. Bacher G, Szymanski WW, Kaufman SL, Zollner P, Blaas D, Allmaier G. Charge-reduced nano electrospray ionization combined with differential mobility analysis of peptides, proteins, glycoproteins, noncovalent protein complexes and viruses. J Mass Spectrom JMS. 2001;36:1038–52.
32. Barlow AL, Macleod A, Noppen S, Sanderson J, Guerin CJ. Colocalization analysis in fluorescence micrographs: verification of a more accurate calculation of pearson's correlation coefficient. Microsc Microanal Off J Microsc Soc Am Microbeam Anal Soc Microsc Soc Can. 2010;16:710–24.
33. Porcel EM, Foose LL, Svitova TF, Blanch HW, Prausnitz JM, Radke CJ. Role of surfactant on the proteolysis of aqueous bovine serum albumin. Biotechnol Bioeng. 2009;102:1330–41.
34. Khandelwal P, Ruiz WG, Apodaca G. Compensatory endocytosis in bladder umbrella cells occurs through an integrin-regulated and RhoA- and dynamin-dependent pathway. EMBO J. 2010;29:1961–75.
35. Eto DS, Gordon HB, Dhakal BK, Jones TA, Mulvey MA. Clathrin, AP-2, and the NPXY-binding subset of alternate endocytic adaptors facilitate FimH-mediated bacterial invasion of host cells. Cell Microbiol. 2008;10:2553–67.
36. Guo X, Tu L, Gumper I, Plesken H, Novak EK, Chintala S, *et al*. Involvement of vps33a in the fusion of uroplakin-degrading multivesicular bodies with lysosomes. Traffic. 2009;10:1350–61.
37. Born M, Pahner I, Ahnert-Hilger G, Jons T. The maintenance of the permeability barrier of bladder facet cells requires a continuous fusion of discoid vesicles with the apical plasma membrane. Eur J Cell Biol. 2003;82:343–50.
38. Fong A, Garcia E, Gwynn L, Lisanti MP, Fazzari MJ, Li M. Expression of caveolin-1 and caveolin-2 in urothelial carcinoma of the urinary bladder correlates with tumor grade and squamous differentiation. Am J Clin Pathol. 2003;120:93–100.
39. Taganna J, de Boer AR, Wuhrer M, Bouckaert J. Glycosylation changes as important factors for the susceptibility to urinary tract infection. Biochem Soc Trans. 2011;39:349–54.
40. Kreft ME, Romih R, Kreft M, Jezernik K. Endocytotic activity of bladder superficial urothelial cells is inversely related to their differentiation stage. Differ Res Biol Divers. 2009;77:48–59.